CONTEMP. PHYS., 1971, VOL. 12, NO. 4, 339–356

Statistical Theories of Melting†

W. G. HOOVER and M. ROSS‡

Lawrence Radiation Laboratory, University of California,
Livermore, California

SUMMARY. Computer experiments can now be used to locate the melting transition for idealized particles which interact according to any specified force law. The results of such computer experiments can then be compared with the predictions of approximate melting theories. We review the computer results obtained for some simple force laws in order to illustrate the successes and limitations of the theories.

1. Introduction

Over the years much literature has been devoted to attempts to predict theoretically the conditions under which a solid will melt or a fluid will freeze.[1] In much of this theoretical work the authors seek a *mechanism* which leads to mechanical instability in the solid or the fluid phase. Solid phase instability can be brought about through the formation of vacancies, by the vanishing of the shear or bulk moduli, or by the spontaneous production of dislocations. Fluid phase instability is signalled by the onset of long-range order or a non-vanishing shear modulus.

Although the study of instability is useful in picturing the *process* of melting, the basic cause of melting has no connection with instabilities. From purely thermodynamic considerations, the fundamental theory of melting can be summarized as

$$T_s = T_f; \quad p_s = p_f; \quad g_s(p, T) = g_f(p, T). \tag{1}$$

The three conditions correspond to thermal equilibrium, mechanical equilibrium and chemical equilibrium. Each of the quantities, temperature, pressure and per-particle Gibbs free energy, must take the same value in the solid phase as in the fluid phase. These equations (1) are melting theory, and describe the three necessary conditions for the two phases to coexist.

The thermal, mechanical and chemical mechanisms for melting are separate complex questions. How do the atoms actually move in going from an ordered phase to a disordered one? The mechanism and the transition rate can depend on the microscopic details of surface structure, imperfections, thermal conductivity and fluid viscosity, all of which vary from one material to another. Thermodynamics is much simpler, for it works in the same way for all materials. It is the thermodynamic aspect of melting we consider here.

If melting theory is so simple, why has so much been written on the subject? It is not that the fundamental theory contains any mysteries but rather that the free energy g is difficult to calculate accurately. A rigorous theoretical free energy calculation for a real material proceeds in two steps, both difficult. First, the crystal structure must be given and the forces with which the atoms or molecules interact must be determined. Second, the macroscopic

† Work performed under the auspices of the U.S. Atomic Energy Commission.

‡ Present address: Theoretical Physics Division, AERE, Harwell, Didcot, Berks., England.

consequences of the forces have to be calculated using statistical mechanics. The two-step calculation has to be carried out separately for each material of interest.

The first step seems to be the harder one. For even the simplest of real materials reliable quantum calculations of interparticle forces in condensed phases have not been carried out. The mathematics of many-body quantum-mechanical systems is still too much for today's computers. The second step of carrying out the many-body statistical mechanical calculations for an assumed force law (even an unrealistic one) was until recently possible only at very high or very low densities. The difficulties in the statistical mechanics were numerical ones and not very severe. These difficulties have now been overcome by using fast computers. Present-day computers can simulate accurately the properties of a few thousand interacting particles. The resulting 'computer experiments' provide accurate thermodynamic properties over the whole density range. The difficulty still remaining is the first one of knowing what the forces in real materials actually are.

The uncertainty in the forces combined with the old difficulties in calculating free energy led to several inexact approaches to a theory of melting. A considerable effort was made to develop theoretical or empirical equations which could describe experimental p,V,T data on melting. The situation can now be clarified. With the computers we can obtain 'experimental' data for a specified force law. When such data, for idealized particles, based on *known* forces, are confronted with the predictions of theory, any disagreement can be ascribed entirely to shortcomings in the theory rather than to uncertainties in the forces. With such a severe test of theories available to suggest further improvements, it is now a particularly appropriate time to review the classical theories and models of melting to see how well they agree with the new computer results.

This study will also allow us to understand what at first appears to be a paradox: we know that melting occurs when the solid and fluid phases are together in equilibrium. Then why is it that melting models based on the properties of only a single phase (as are all the instability models) can successfully describe a *two-phase* phenomenon in which solid and fluid are equally important?

2. Melting for inverse power potentials

The simplest possible idealization of intermolecular forces which is still complicated enough to show a melting transition is derived from the inverse power potential:

$$\phi(r) = \epsilon(\sigma/r)^n. \tag{2}$$

The particles are point centres of repulsion, with the force on any particle being a vector sum of contributions $-\mathrm{d}\phi/\mathrm{d}r$ from all the other particles. The strength of the interaction is proportional to the microscopic energy ϵ. The 'diameter' of the particles is the length σ. The hardness or stiffness of the particles increases with n.

We will consider specifically the three most commonly used values of n, 4, 12 and ∞. The corresponding pair potentials are shown in fig. 1.

The very soft ($n=4$) case of 'Maxwellian molecules' and the very hard ($n=\infty$) case of 'hard sphere' particles are not especially realistic, but both

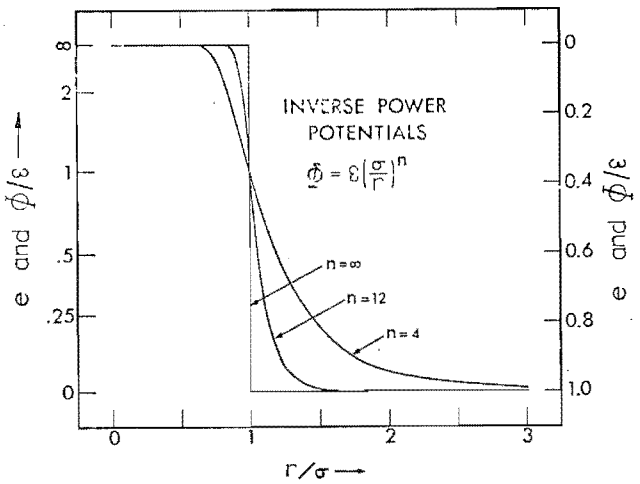

Fig. 1. Inverse power pair potentials. Maxwellian molecules correspond to $n=4$; hard spheres to $n=\infty$.

have been studied since the time of Maxwell and Boltzmann because their transport coefficients and equilibrium properties were the easiest to calculate theoretically. An intermediate value ($n=12$) provides a more realistic description of actual repulsive forces between closed electron shells. This potential, the 'soft-sphere' potential, is the high-temperature limit of the much-studied Lennard-Jones potential, which has been successfully applied to the description of the rare gases.

For any of the inverse power potentials the thermodynamic and transport properties are particularly easy to calculate because once a single isotherm, isochore or isobar is known all the others can be determined from it. For the thermodynamic properties this follows from the way that the configurational Helmholtz free energy depends on density and temperature. The Helmholtz free energy function $H=U-TS$, rather than the Gibbs free energy function $G=U+pV-TS=H+pV$, is more convenient in statistical calculations[2] because volume (rather than pressure) is the fundamental independent variable in theoretical calculations. From statistical mechanics the dependence of the Helmholtz free energy on the volume and temperature is given by the canonical partition function $Z_N(V, T)$:

$$Z_N = \exp(-H/kT) = \frac{1}{N!\,\Lambda^{3N}}\int \exp\left(-\sigma^n \frac{\epsilon}{kT}\sum r_{ij}^{-n}\right) d\mathbf{r}^N$$
$$= \frac{V^N}{N!\,\Lambda^{3N}}\int \exp\left(-\rho^{n/3}\frac{\epsilon}{kT}\sum s_{ij}^{-n}\right) d\mathbf{s}^N \qquad (3)$$

where

$$\rho \equiv N\sigma^3/V; \quad \mathbf{s} \equiv \mathbf{r}(N/V)^{1/3}; \quad \text{and} \quad \Lambda^2 \equiv h^2/(2\pi mkT).$$

The sums in (3) range over all $N(N-1)/2$ pairs of particles. The reduced distances $\{s\}$ have been introduced to show that the non-ideal part of the free energy, given by the integral multiplying $V^N/(N!\,\Lambda^{3N})$ in (3), depends only on the single density-temperature variable $x=\rho(\epsilon/kT)^{3/n}$, rather than on V and T separately. This remarkable simplification of the partition function occurs only for inverse power potentials.

The dimensionless thermodynamic properties obtained by differentiating the partition function ($\mathrm{d}H = -p\mathrm{d}V - S\,\mathrm{d}T$)—that is, pV/NkT, U/NkT and $(S-S_{\mathrm{ideal}})/Nk$—likewise depend only on the combined density-temperature variable x. Thus any isotherm or isochore, over which $\rho(\epsilon/kT)^{3/n}$ varies from 0 to ∞, gives the entire equation of state for all V and T.[3]

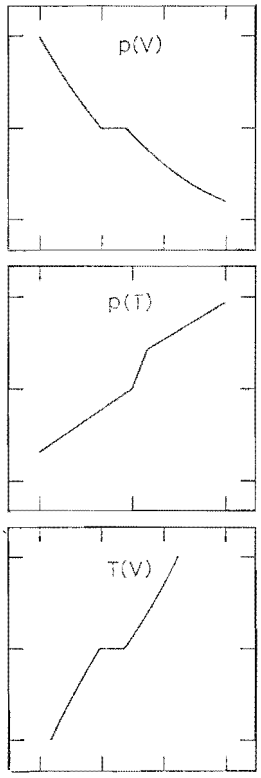

Fig. 2. Variation of pressure, volume and temperature in the vicinity of the melting and freezing transitions. The numerical results on which these curves are based were obtained using the inverse twelfth power potential.

Along any isotherm, isochore or isobar the melting transition is characterized by two discontinuities, as shown in fig. 2. $(\partial p/\partial V)_{\mathrm{T}}$, $(\partial/p\partial T)_{\mathrm{V}}$ and $(\partial T/\partial V)_p$ all are discontinuous at melting and again at freezing. The discontinuities, which signal the start and the finish of melting, occur at two characteristic values of the density-temperature variable x:

$$x_{\mathrm{s}} \equiv \rho_{\mathrm{s}}(\epsilon/kT)^{3/n}; \quad x_{\mathrm{f}} \equiv \rho_{\mathrm{f}}(\epsilon/kT)^{3/n}, \tag{4}$$

where ρ_{s} and ρ_{f} are the densities of the coexisting melting solid and freezing fluid at temperature T. If we introduce z_{s} and z_{f} for the corresponding pure-phase compressibility factors, $(pV/NkT)_{\mathrm{s}}$ and $(pV/NkT)_{\mathrm{f}}$ in the solid and fluid phases, then the three pVT relations at melting can be expressed in terms of the x_{i} and z_{i} (where i stands for either s or f):

$$\begin{aligned} p\sigma^3/\epsilon &= \rho^{(n+3)/3}\, z_{\mathrm{i}} x_{\mathrm{i}}^{-n/3}\,; \\ p\sigma^3/\epsilon &= (kT/\epsilon)^{(n+3)/n}\, z_{\mathrm{i}} x_{\mathrm{i}}\,; \\ \rho_{\mathrm{i}} \quad &= (kT/\epsilon)^{3/n}\, x_{\mathrm{i}}. \end{aligned} \tag{5}$$

The constants characterizing the melting transition, x_s, x_l, z_s and z_l have to be determined from statistical calculations.

The exact (for inverse power potentials only!) relations in (5) suggest a number of empirical macroscopic pVT relationships at melting. The Simon pT relation[4] between the melting pressure and temperature,

$$(p-p')/a=(T/T')^c-1, \tag{6}$$

has long been used to extrapolate to high pressure–high temperature melting conditions (such as those within the earth) which are experimentally inaccessible. For the inverse power potentials the Simon equation is exact, and the constant c is $(1+3/n)$. The simple relations (5) for the inverse power potentials appear first to have been pointed out by Domb.[5] Although the inverse power approximation is useful for real materials over a limited density range, we know that real materials are likely to show decreasing values of n, and therefore increasing values of c, at high compression. Consequently the Simon equation cannot be trusted at high compressions. It tends to overestimate the temperature at which melting occurs.

An approximate VT melting relation states that the volume expansion at melting, relative to the initial standard volume V', is a linear function of temperature:[6]

$$T/T'=1+c(\Delta V/V'). \tag{7}$$

This appears to be the first two terms of a power series expansion in $(\Delta V/V')$. For inverse power potentials, it is. The full expansion follows from (4):

$$T/T'=1+\frac{n}{3}(\Delta V/V')+\frac{n(n+3)}{18}(\Delta V/V')^2+\ldots. \tag{8}$$

In the inverse power case we see that the expansion converges poorly for large n, corresponding to steep repulsion. Even for the softest case, a Maxwellian solid ($n=4$), the third term increases to 5 per cent of the second term by the time the solid has been compressed 4 per cent. Evidently (7) should fail badly at high compressions, predicting, unlike the Simon equation, too low a temperature at melting. If the effective value of n changes rapidly with compression this change can compensate for the higher terms omitted in (7). Grover [7] has shown that such a compensation actually occurs for alkali metals, where (7) reproduces experimental data for $\Delta V/V'$ up to 0·4. However (7) has *not* been shown to be successful in predicting melting beyond $\Delta V/V'\approx 0{\cdot}1$ for any other class of materials. It fails in the case of closed shell systems such as the rare gases and ionic solids (where n is known to be of order 9 or more) and has not been adequately tested for non-alkali metals because of a lack of data.

An underlying microscopic simplicity is responsible for the many simple macroscopic relations among inverse-power thermodynamic quantities. We have already introduced the scaled distances $\{s\}$, giving lengths in units of the characteristic length $(V/N)^{1/3}$. An immediate consequence of this step is the observation that the relative importance of any configuration in scaled space is always the same at fixed $\rho(\epsilon/kT)^{3/n}$. This can be seen most easily from the dynamical point of view. If we also introduce scaled time, τ, measured in units of the characteristic time $(V/N)^{1/3}(m/kT)^{1/2}$, the scaled equations of motion for inverse power particles are simplified. The scaled accelerations,

$d^2s/d\tau^2$, and forces are found to depend only on the density-temperature variable x. This means that for a fixed value of $\rho(\epsilon/kT)^{3/n}$, the dynamic behaviour of the system in s–τ variables at any density or temperature looks exactly the same. On the time-averaged basis of statistical mechanics, this dynamical identity shows again that the relative importance of any configuration of particles, expressed in s coordinates, is density and temperature independent at fixed $\rho(\epsilon/kT)^{3/n}$.

Because melting and freezing occur at characteristic values of x, each possible configuration in the scaled coordinates will always have the same probability, and the scaled ' structure ' of the solid and fluid along curves of constant x will always be the same. In pictorial language we can say that as we move along the melting or freezing curve all the atoms in the solid or fluid will always be in the same relative positions to one another when viewed in the scaled space. Therefore, because the relative arrangements are unchanged, any x-dependent structural characteristic, when expressed in scaled variables, can serve as an indicator of melting or freezing.

The best-known example of a structural characteristic used to predict melting is the solid-phase Lindemann law,[8] which states that the ratio of the root-mean-squared displacement to the nearest-neighbour spacing is a constant along the melting line. Because the characteristic length used in defining our reduced distances was $(V/N)^{1/3}$ and is essentially the nearest-neighbour spacing, the Lindemann ratio is a *scaled* root-mean-squared displacement and must be constant at fixed $\rho(\epsilon/kT)^{3/n}$. For any inverse power potential *any* function of the s variables is constant along the melting line so that the Lindemann relation is exactly correct.

In the fluid, particle displacements are no longer a useful structural description. Instead, the pair distribution function is introduced. It gives the probability, relative to the ideal-gas probability, of finding two particles a distance r apart. In scaled variables the pair distribution function in the freezing fluid is constant along the freezing line. The Fourier transform (called the structure factor) of the pair distribution function is often discussed instead, because a portion of the transform can be directly measured in laboratory experiments designed to scatter x-rays or neutrons from the fluid. For inverse power potentials the scaled Fourier transform is unchanged along the freezing line. Because the actual structure factor is a function of the wave-vector $\vec{\mathbf{k}}$, an inverse length, the characteristic positions of extrema in the structure factor vary as $\rho^{1/3}\propto(kT/\epsilon)^{1/n}$ at freezing. Ashcroft and co-workers[9] have correlated the freezing densities for liquid metals using a structure-factor criterion. This is the analogue, for fluids, of Lindemann's law.

Ross[10] introduced a criterion for melting closely related to the scaling of the microscopic particle distributions. He predicted that the non-ideal part of the Helmholtz free energy would be constant along the melting line. This constancy follows from the form of the partition function in (3) and also from the dynamical analysis showing that the relative importance of the scaled configurations contributing the excess free energy depends only on x.

The simple scaling relations for the dynamics, the macroscopic thermodynamics, the Lindemann constant, the structure factor, and so on are *not* obtained if attractive forces are added to the inverse power repulsion or if the repulsion has some other form. The microscopic structure in real systems

actually does change somewhat along the melting line, and it is therefore necessary to calculate separately the variation of the free energy with volume at each temperature. We expect, however, that over a limited density-temperature range the inverse-power model can be used to describe real materials. The fact that several empirical melting relations hold exactly for inverse power particles supports the analogy.

The fact that the microscopic structure in both phases, solid and fluid, scales in the same way as does the melting transition, a two-phase property, explains the apparent paradox mentioned in the Introduction, namely that one-phase properties adjusted to fit a single point (thus determining $\rho(\epsilon/kT)^{3/n}$) on the melting line can be successfully used to predict the whole curve. We see now that such predictions would be *exact* for an inverse power potential. The validity of the scaling for real materials still must be determined.

3. Results from the computer experiments

The Maxwellian, soft-sphere and hard-sphere potentials have all been studied in computer experiments. The results of such calculations differ from results of laboratory experiments primarily in that the forces are chosen in advance in computer experiments.

Ordinarily periodic boundaries are used, as shown in fig. 3, to eliminate number-dependent surface effects. In the computer experiments a large number of equilibrium configurations is generated (typically a few hundred thousand), either by the molecular-dynamic method[11] of solving the classical equations of motion or by the simpler ' Monte Carlo ' procedure.[12]

In Monte Carlo calculations velocities are absent; the particles proceed from one configuration to another, not according to $\boldsymbol{F}=m\ddot{\boldsymbol{r}}$ but as a result of random moves. By selecting all such moves which lower the potential energy Φ, but only a fraction $exp\,(-\delta\Phi/kT)$ of those moves which increase the energy by $\delta\Phi$, the Monte Carlo method generates exactly the same configurations that would occur if the equations of motion were solved instead. As the configurations are generated, the pressure and the energy are calculated as averages. Typical results are shown in fig. 4 for the Maxwellian,[13] soft-sphere[14] and hard-sphere[15] particles.

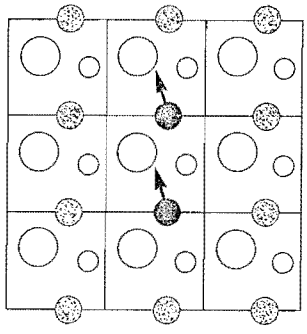

Fig. 3. Schematic illustration of the periodic boundaries used to eliminate surface effects in computer calculations. The system shown contains three particles and is surrounded by periodic replicas of the same system. Notice that the dark particle, just leaving the central cell, is being replaced by its periodic image (the other images of this particle are lightly shaded). The number of particles in the central cell is constant.

A peculiarity of the computer experiments is that they cannot easily handle coexisting phases. This is because the relatively large fraction of particles, of order $N^{-1/3}$, on the two-phase boundary where the phases meet is negligible only for systems much too large to study with computers. The inhomogeneous surroundings in the vicinity of a phase boundary cause the surface particles to have a higher free energy than that in either pure phase. The free energy increase due to the surface particles makes the computer results in two-phase regions depend strongly on the number of particles.[16] In contrast, the one-phase results (where surface effects have been eliminated by using periodic

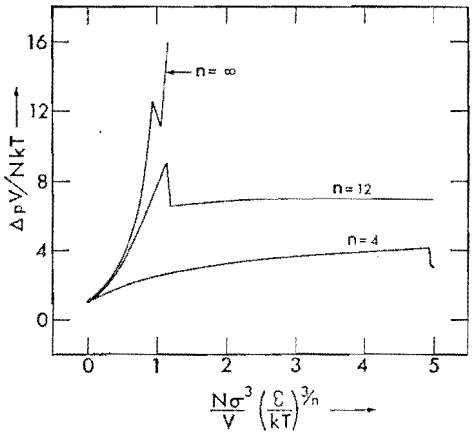

Fig. 4. Thermodynamic equations of state for three inverse power potentials from computer experiments. $\Delta pV/NkT$ is the increase in the compressibility factor over that of a perfect static lattice at the same density and temperature. The discontinuities in the slopes of the three curves correspond to the melting and freezing transitions.

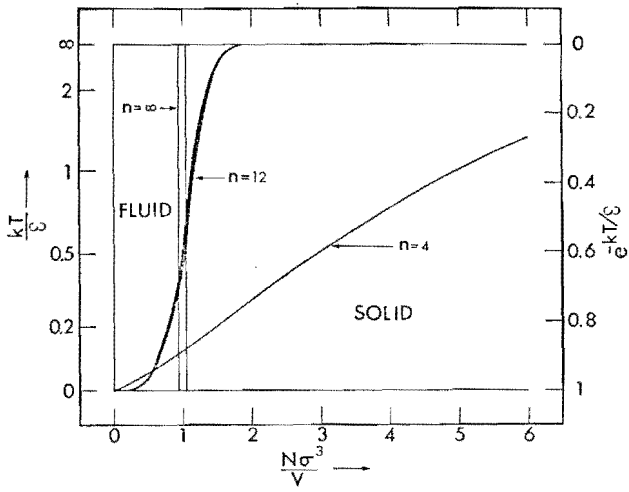

Fig. 5. Boundaries of the two phases, fluid and solid, for inverse power potentials. The narrow strips (clear for $n=\infty$ and black for $n=12$) correspond to the two-phase region where fluid and solid can coexist. This region is very narrow for the softer Maxwellian molecules ($n=4$).

boundaries) depend only a little on system size so that separate free energy calculations for the two phases can accurately predict the phase transition location corresponding to the ' thermodynamic limit ', $N \to \infty$.

To locate the melting transition, the computer pressure or energy data for the two phases have to be integrated to get the free energy. The Helmholtz free energy for each phase can be determined by either a volume or a temperature integration:

$$(\partial H/\partial V)_T = -p; \quad (\partial [H/T]/\partial T)_V = -U/T^2. \tag{9}$$

Then the phase boundaries, along which the solid and fluid temperature, pressure and per particle Gibbs free energies are equal, can be determined.[17] The phase boundaries determined in this way for the three inverse power potentials are shown in fig. 5. Notice that, as predicted by the scaling relations (4), the hard-sphere melting and freezing densities are temperature independent. The corresponding densities for soft-sphere and Maxwellian particles are respectively proportional to $T^{1/4}$ and $T^{3/4}$.

All three inverse power potentials have been studied at Livermore.[13–15] The hard-sphere results agree quantitatively with independent work carried out at Los Alamos.[18] The soft-sphere results agree with calculations done at Orsay.[19]

Although the inverse power potentials are the simplest to use, they are not sufficiently realistic at low temperatures where attractions must be taken into account. Attractions split the fluid portion of the phase diagram into two parts, gas and liquid. These same attractive forces spoil the simple scaling of the forces and of the melting equations, complicating the computer experiments designed to map out the phase diagram. The most extensive work carried out so far represents the attractive part of the potential by adding on an inverse sixth power attraction to the soft-sphere repulsion:

$$\phi_{LJ}(r) = Ar^{-12} - Br^{-6}. \tag{10}$$

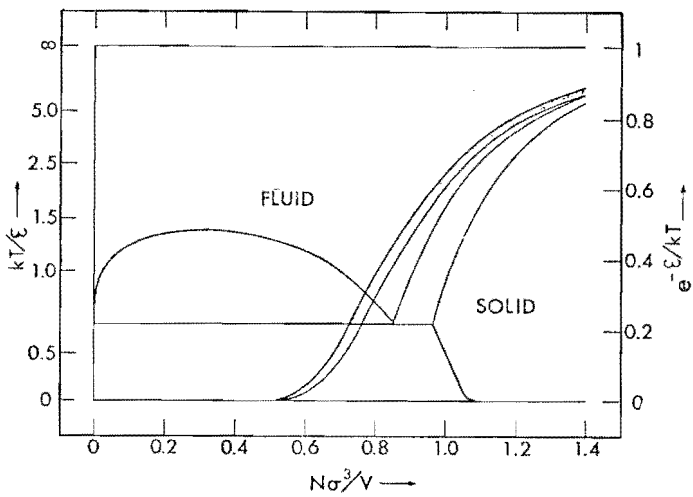

Fig. 6. The Lennard-Jones phase diagram, as determined at Orsay and Los Alamos. Superimposed on this diagram is the soft-sphere phase diagram resulting when only repulsive forces are used. The fluid–solid two-phase region for the soft-sphere potential is lightly shaded.

For this 'Lennard-Jones' potential the entire equation of state has been determined, mostly at Orsay,[20,21] but with considerable corroborating calculations from Los Alamos.[18] At pressures up to about two kilobars the computer results fit closely the measured results of laboratory experiments on solid and fluid argon, so that at moderate pressures the potential (10) is probably fairly close to the true interaction between argon atoms. This correspondence illustrates that the fundamental problem of determining intermolecular forces can be attacked more easily by comparing calculated thermodynamic properties with experiments than by attempting to carry out accurate quantum mechanical calculations of the forces.

The Lennard-Jones density-temperature phase diagram, shown in fig. 6, has superimposed on it the phase diagram for the soft-sphere repulsive potential. The similarity suggests that where the deviations are small the effect of the attractive forces could be treated by first-order perturbation theory. A 'first-order' theory assumes that the particle distribution is unchanged by the presence of the attractive term. A 'second-order' theory would calculate the changes in the distribution too. The first-order change in Helmholtz free energy is found by averaging the contributions of the sixth-power term, using the distribution found for the repulsive twelfth-power alone. In first-order theory the change in Helmholtz free energy is

$$\Delta H = (N^2/2V)\int(-Br^{-6})g_0(r)\,\mathrm{d}\boldsymbol{r}, \tag{11}$$

where $g_0(r)$ is the pair distribution function based on the repulsive forces. The first-order changes in energy and pressure can be derived by differentiating ΔH with respect to T and V. The resulting expressions[20] involve not just the pair distribution function $g_0(r)$, but also the three- and four-particle distribution functions. Hansen has carried out the complete first-order perturbation calculation for both the fluid and the solid phases. His results show that the first-order correction (11) is adequate only at temperatures well above the critical temperature. Thus any fundamental theory based on free energy calculations from perturbation theory is restricted to high temperatures.

Nevertheless it is possible that certain average properties other than pressure and energy are less sensitive to attractive forces and so can be used to follow the melting transition to low temperatures. Hansen found that the Lindemann ratio, $\langle r^2\rangle^{1/2}/d$, where d is the nearest-neighbour spacing, remained constant within its statistical error (5 per cent) over a temperature range from the triple point to the high-temperature soft-sphere limit. In the fluid phase the corresponding indicator of freezing, the principal maximum in the structure factor, was likewise found to be nearly temperature-independent within its statistical error (2 per cent).

These two characteristic functions for melting and freezing illustrate that relations which are exact for simple inverse power potentials can be *effectively* correct for more complicated situations, and therefore useful in analysing real experimental data. In describing real materials, with unknown forces, the first step is to determine an effective pair potential by analysing experimental data. Then the statistical theory, using the same potential, can be applied to phase-diagram calculations.

4. Approximate theoretical models

To save the expense of actual computer calculations, theoretical models for the thermodynamic or structural properties of the solid and fluid phases are useful. In order to apply such models to real materials some force law must be chosen, consistent with experimental data. Given the forces the models can be applied. The most fundamental approach to melting is a free energy comparison between the two coexisting phases. The approach becomes a ' model ', rather than exact statistical mechanics, only because the free energy calculation is approximate.

The most successful theory so far devised for fluid-phase free energy is based on finding the hard-sphere diameter which best represents, in the sense of minimizing the first-order perturbation theory Helmholtz free energy, the softer potential of interest.[22] This theory predicts pressures and energies in terms of the hard-sphere free energy (which is already known from computer experiments) and the hard-sphere distribution function (which can be approximated fairly well by the Wertheim-Thiele solution of the Percus-Yevick integral equation). If the repulsive portion of the soft potential is reasonably steep, r^{-12} for example, then this theory works well, with errors in the free energy of order $0{\cdot}3NkT$. For softer potentials such a perturbation approach would have to be based on a softer unperturbed potential.

In the solid phase the hard-sphere distribution is not available in a convenient form for numerical work. Instead the Lennard-Jones–Devonshire cell model is used to make an estimate of the thermodynamic properties.[23] According to this cell model the partition function is approximated by the Nth power of a one-particle integral in which a ' wanderer ' particle moves in the energy field of all the others. All particles but the wanderer are assumed fixed at their lattice sites. The cell version of the partition function is:

$$Z_{\text{cell}} = \exp\left(-\Phi_0/kT\right)\left[\Lambda^{-3}\int_{\Delta} \exp\left(-\delta\Phi/kT\right) \mathrm{d}\boldsymbol{r}\right]^N \tag{12}$$

where the potential energy of the perfect stationary lattice is Φ_0. The change in the potential energy of the system when the wanderer moves away from its lattice site to $\boldsymbol{r}$ is $\delta\Phi$. The Δ next to the integral indicates that the wanderer is not allowed to leave its cell. This model predicts accurately the energy and the pressure in the solid phase, but is less accurate in predicting free energy. The free energy errors are about the same order of magnitude, at melting, as are the fluid-phase perturbation theory errors at freezing, $0{\cdot}3NkT$.

Another approach to solid-phase thermodynamics is more traditional but no more accurate. This is via lattice dynamics.[24] The potential energy of the crystal is expanded in powers of the displacements of the particles from their lattice sites. If terms higher than quadratic are ignored (which is justified at low enough temperatures) the motion of a periodic crystal with fixed centre-of-mass can be analysed into $3N-3$ normal-mode vibrations, each with a characteristic frequency ν. The partition function for such a crystal becomes the product of $3N-3$ harmonic oscillator partition functions,

$$Z_{\text{harmonic}} = \exp\left(-\Phi_0/kT\right)\prod kT/h\nu. \tag{13}$$

At higher temperatures, near melting, the anharmonic corrections ignored in (13) become so large that the harmonic free energy is no more accurate

than is the cell model free energy. The best guess for the free energy of the solid would be based on the low temperature free energy from (13) with an anharmonic correction based on the cell model (12).

Although perturbation theory, the cell model and lattice dynamics all calculate free energy, in principle the correct way to locate a phase transition, the small errors these models make in free energy lead to larger errors in the transition pressure and density. A free energy error of $0{\cdot}3NkT$ in either phase would change the calculated hard-sphere transition pressure by about 25 per cent, for example. Because phase transitions are sensitive to small free energy changes it is in practice worth while to consider simpler one-phase theories, less fundamental but just as accurate. We will describe three such models; compare their predictions with computer experiments; and then go on to show that these models are useful in interpreting real data from laboratory experiments.

A model for melting based on the Lennard-Jones–Devonshire cell model makes use of the scaling property found for the inverse power potential in (3). In the cell-model approximation the reduced one-particle integral, v_f^*, a scaled free volume, can be introduced by using the reduced distance $\mathbf{s} \equiv \mathbf{r}(N/V)^{1/3}$:

$$Z_{\text{cell}} = \exp(-\Phi_0/kT)(V/N\Lambda^3)^N v_f^{*N};$$

$$\exp(-H_e/NkT) = v_f^* \equiv \int_\Delta \exp(-\delta\Phi/kT)\,\mathrm{d}\mathbf{s}, \tag{14}$$

where H_e is the Helmholtz free energy relative to that of an ideal gas particle confined to the volume V/N in a mean field equal to the static lattice energy.

Proceeding by analogy with the inverse power results we *assume* that the single-particle free volume v_f^* is constant along the melting curve. Despite its approximate basis this assumption would *exactly* reproduce the melting curve for an inverse power potential. To the extent that v_f^* is constant as the inverse power varies we can expect that more general potentials could be described with the same v_f^*.

The best test for this approximate model is given by the Orsay data for the Lennard-Jones potential.[21] We have carried out calculations of v_f^* for this potential at the same temperatures for which the melting density has been determined. Using the soft-sphere value of v_f^* (melting), 0·0041, we have found numerically the density at which the Lennard-Jones potential has the same value of v_f^* at the lower temperatures. The results of this calculation are shown in table 1, compared with the actual Monte Carlo results of Hansen and Verlet. The excellent agreement, at temperatures as low as the triple point, confirms the notion that selected averages can be insensitive to the presence of attractive forces. The scaled free volume, which is an average over all the arrangements of a particle in its cell, is evidently a good choice. We would expect equally good agreement for any reasonable pair potential. The fact that the agreement is not so good at low temperature points out the need to determine melting law parameters at the highest possible pressures. Doing so minimizes the complications introduced by the attractive forces.

A second one-phase melting model can be derived from a modified 'correlated' cell model which incorporates a physical mechanism for solid-phase instability. The model is illustrated in fig. 7. Two of the neighbours of the wanderer move co-operatively with it so that the resulting motion

corresponds to a long wavelength shear wave. Such a model was used by Squire and Salsburg[25] with somewhat surprising results. In two dimensions the model accounts for the observed first-order melting transition found for hard discs.[26] The model predicts a van der Waals loop at approximately the same pressure and density as is found in computer experiments carried out on several hundred discs.[27] In three dimensions, however, the model does not predict a loop, thus failing to account for the well-established hard-sphere melting transition. The good agreement for discs must therefore be regarded as somewhat fortuitous.

Table 1. Comparison of predicted melting densities (scaled) for the Lennard-Jones potential with the Monte Carlo results from Reference 21. The predictions are based on matching the cell model v_f^* at each temperature to the v_f^* found empirically to fit the soft-sphere data of Reference 14. The densities given in this table, $N\sigma^3/V$, apply to the Lennard-Jones potential in the form $4\epsilon[(\sigma/r)^{12}-(\sigma/r)^6]$.

kT/ϵ	Monte Carlo ρ_s	Predicted ρ_s
100	2·71	2·71
2·74	1·18	1·19
1·35	1·05	1·04
1·15	1·02	1·01
0·75	0·97	0·94

Applying the same correlated cell model to the soft-sphere potential we found a maximum in the molar heat capacity, C_v. This maximum is of special interest because it occurs without invoking vacancy formation. The maximum occurs at the density where the wandering central particle can first approach the edge of its cell. Such a motion evidently corresponds to the diffusion of atoms through the solid. Because such a motion is mechanical instability, rather than melting, the break-up of the crystal occurs at a lower density than the melting density. However, because the instability occurs in the vicinity of melting, it can be used as a rough guide.

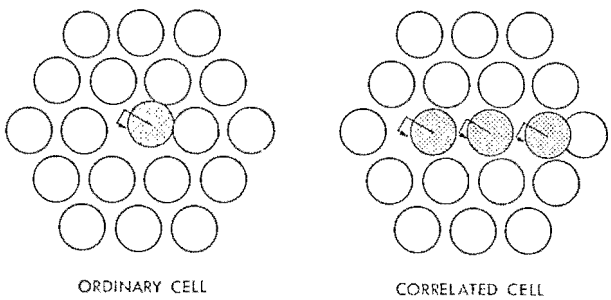

Fig. 7. Comparison of the ordinary cell model, in which the central particle moves in the field of its fixed neighbours, with the correlated cell model, in which two of the neighbours (those which would be closest and farthest away in the ordinary cell model) move along with the central particle.

In fig. 8 the form of the 'specific heat anomaly' (the anomaly in C_v) is shown at three different temperatures for the Lennard-Jones potential. For argon the highest temperature point corresponds to 12 000 K. The other temperatures are twice critical and the triple-point temperature. There is a good semiquantitative correspondence between the 'knee' in the molar heat capacity and the density of the freezing fluid. Because the 'specific heat anomaly' found in the cell model is produced by the sliding of particles past one another, corresponding to mechanical instability, this model indicates that the instability density and the freezing density roughly correspond at all temperatures. Both scale along the melting line.

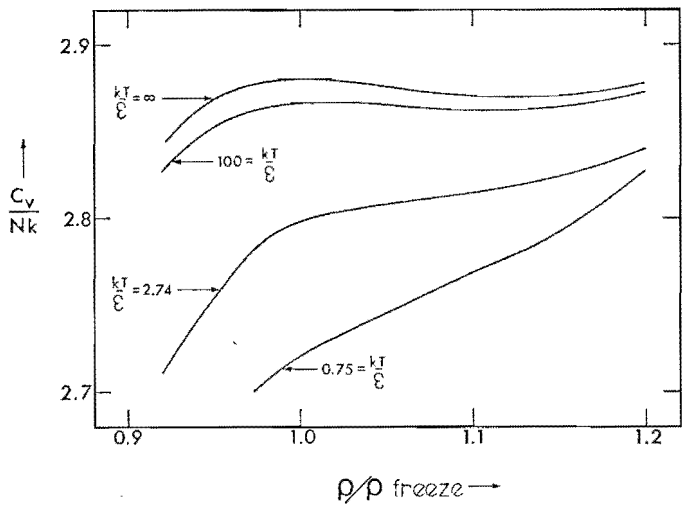

Fig. 8. Molar heat capacity C_v as obtained from the correlated cell model in the vicinity of the melting and freezing transitions. The four curves cover a temperature range from ∞ down to the normal liquid. Note that all four curves exhibit a maximum or a 'knee' in the vicinity of freezing.

An analogue of mechanical instability can be found in the computer calculations in the vicinity of melting, and can be used as a third melting model. If the density is gradually decreased in the computer experiments a well-defined density is found at which diffusion first sets in and the solid-phase ordered structure breaks down. This density can be determined accurately with only a little machine calculation. Ross and Alder suggested that this computer instability density should correspond to the freezing density of the fluid, arguing that any density at which the fluid can form in a computer experiment ought to correspond to pure fluid in the thermodynamic large-system limit. Using the maximum melting density criterion Ross and Alder[28] determined a high-temperature melting curve for argon. The soft-sphere results indicate that their estimates for the freezing density will be too low, by about 4 per cent, at high temperature. The actual scaled freezing density, x_f, is 1·150. In the computer calculations a 32-particle solid melted at 1·089, but at 1·131 a 500-particle solid did not melt even after 1·1 million moves.

We made a number of instability-point runs for the full Lennard-Jones potential, determining the density at which the 108-particle solid no longer melts after a run of one million moves. (The averages between the lowest density at which the solid did not melt and the next lower density were actually used.) For the soft-sphere potential the instability density is $(1{\cdot}131 + 1{\cdot}089)/2 = 1{\cdot}110$. The Lennard-Jones results are shown in table 2 compared with the actual melting densities. The ratios of the two sets of numbers are remarkably

Table 2. Comparison of melting instability densities (scaled) for the Lennard-Jones potential. The instability density corresponds to the highest density at which the solid phase, in an N-particle periodic system, spontaneously melts.

kT/ϵ	ρ_m	ρ_i	ρ_m/ρ_i	N
∞[a]	$0{\cdot}844(kT/\epsilon)^{1/4}$	$0{\cdot}785(kT/\epsilon)^{1/4}$	1·075	32; 500
100	2·706	2·468	1·096	108
2·74	1·179	1·058	1·114	108
1·06	1·012[b]	0·899	1·126	108
		Average:	1·103	
Hard-spheres	1·041	0·943	1·104	500

(*a*) This high-temperature limit for the Lennard-Jones potential is based on the soft-sphere r^{-12} repulsion.[14],[19] The densities quoted, $N\sigma^3/V$, apply to the Lennard-Jones potential in the form $4\epsilon[(\sigma/r)^{12}-(\sigma/r)^6]$.

(*b*) Obtained by interpolating the results of Hansen and Verlet.[21]

constant. The reason must be that although the instability observed in the computer experiments is *not* the melting transition but a different structural instability, it scales in the same way as does the melting transition. Although, strictly speaking, the instability density will eventually, for extremely long runs on very large systems, coincide with the melting density, so that the ratio will drop to unity, the change of instability density with system size and length of run is so small that the instability density in practice is quite reproducible, barely changing even for the largest systems computers can study.

The hard-sphere ratio, given in the last row of table 2, agrees with the soft-sphere estimate, suggesting that the 10 per cent difference between the melting and instability densities is fairly general. This suggests that the extensive Monte Carlo calculations required to find the melting point could be circumvented by finding the break in the solid-phase isotherm and multiplying the corresponding density by 1·1. A solid-phase calculation at this density followed by a fluid phase calculation at the same pressure would then provide the melting parameters. These calculations could be carried out with satisfactory accuracy using the Mansoori–Canfield perturbation theory for the fluid pressure and the Lennard-Jones–Devonshire cell model for the solid.

To make the two cell models and the instability model just discussed more relevant to real experiments, not just computer experiments, let us apply these

ideas to argon. An effective intermolecular pair potential for argon has been determined by fitting shock-wave experiments in which the liquid is compressed from 28·4 $cm^3\ mol^{-1}$ to 9·7 $cm^3\ mol^{-1}$; the temperature rise is about 12×10^3 K.[29] (These compressed conditions correspond to a soft-sphere density-temperature variable $x = 1{\cdot}0$.) The pair potential is of the exponential-six form:

$$\phi(r) = \epsilon\left[\frac{6}{\alpha-6}\exp\{\alpha(1-r/r^*)\} - \frac{\alpha}{\alpha-6}(r^*/r)^6\right];$$
$$\alpha = 13{\cdot}5; \quad r^* = 0{\cdot}385 \text{ nm } (= 3{\cdot}85 \text{ Å}); \quad \epsilon/k = 122 \text{ K}. \tag{15}$$

Ross and Alder have used this pair potential to calculate Monte Carlo isotherms and used the breaks in the isotherms to locate the melting point. Their agreement appears to have been fortuitous, since the change in density on freezing at the temperature they chose to compare with experiment was about 9 per cent, quite close to the 10 per cent increase in density on going from the instability point to the melting point. The estimates of the instability densities from these isotherms, multiplied by 1·1, are shown in the second column of table 3. These are our estimates of the melting densities. In the third column are some experimental results, expressed in the same units. The fourth column in table 3 is analogous to the third column in table 1. We have

Table 3. Comparison of predicted melting densities (scaled) for argon using the exponential-six potential. The second column shows the instability densities multiplied by 1·1 (predicted melting densities). The third column shows the experimental melting densities. The last column shows the melting densities predicted using a constant value of v_f^* chosen to fit the experimental density at 322 K. The densities in this table are defined by $\rho = N r^{*3}/\sqrt{(2)}V$, using the potential parameters appearing in (15).

T/K	$1{\cdot}1\rho_i$	ρ_m	$\rho_m\ (v_f^*)$
108	1·01	1·013[a]	0·983
201	—	1·121[a]	1·121
322	—	1·253[b]	1·253
2 440	2·28	—	2·31
12 200	4·55	—	4·56

(*a*) R. K. Crawford and W. B. Daniels, 1968, *Phys. Rev. Letters*, **21**, 367.
(*b*) Reference 30.

used (14) for v_f^* and the potential (15) to determine those densities at which v_f^* is the same as that corresponding to the 322 K measurement of Stishov *et al.* on argon.[30] This scaling, based on the cell-model free volume, covers the entire range of experiments and Monte Carlo calculations to the same accuracy as the corresponding calculation using the Lennard-Jones potential. We chose to use the 322 K point as the basis for this calculation because it was the highest-pressure point available, and should therefore minimize the effect of the attractive forces. We used an experimental point rather than a Monte Carlo point because the experimental point is more accurate.

Table 4. High-temperature melting curve for argon. The theoretical predictions are based on the exponential-six potential and the v_f^* cell-model scaling chosen to fit the experimental volume at 322 K.

T/K	V/cm^3 mol^{-1}	p/kbar	V_{theory}/ cm^3 mol^{-1}	p_{theory}/ cm^3 mol^{-1}
201·32[a]	21·69[a]	6·34 (0·01)	21·70	6·13
322[b]	19·4[b]	15·84 (0·02)	19·40	15·39
400	—	23[c] (0·5)	18·36	22·44
420	—	26·3[c] (2)	18·13	24·37
450	—	—	17·80	27·35
500	—	—	17·30	32·53
600	—	—	16·45	43·69
800	—	—	15·15	68·83
1 000	—	—	14·16	97·37
1 500	—	—	12·45	181·75
2 000	—	—	11·30	282·68
2 440	—	—	10·53	383·92

(*a*) R. K. Crawford and W. B. Daniels, 1968, *Phys. Rev. Letters*, **21**, 367.
(*b*) Reference 30.
(*c*) J. D. Grace and G. C. Kennedy, 1966, *J. Phys. Chem. Solids*, **28**, 635.

In table 4 we have used the same theory to predict additional points along the argon melting curve up to 2440 K. In the second and third columns are some experimentally determined volumes and pressures. The fourth and fifth columns display the theoretical predictions. At 6 kilobar and 15 kilobar the theoretical predictions for the pressure are low by 3 per cent (about the error one might expect based on uncertainties in the potential and in the cell model). The only serious discrepancy with existing measurements appears at 420 K. However, Professor Kennedy has informed us that the uncertainty of this point, the highest pressure point in an extensive series, may be as large as 2 kilobar. That this would appear to be so is borne out by the good agreement between our calculations and a nearby experimental point at 400 K.

These calculations have used idealized pair potentials which are most applicable to rare gases or spherical molecules. However, from the point of view of the theorist, melting theory in other materials is in principle no more complicated. With the computers and melting models now available melting theory reduces to the question of finding good 'effective pair potentials' or, even more simply, good effective repulsive pair potentials.

Acknowledgments

We would like to thank Warren G. Cunningham for his help with the Livermore computing machinery and Roger McLain for drawing the illustrations.

Notes and References

(1) An excellent review of experimental data together with phenomenological and theoretical treatments of melting can be found in a book by A. B. Ubbelohde, *Melting and Crystal Structure* (Oxford: Clarendon Press, 1965).

(2) In principle, and even in practice, calculations with other independent variables, P and T, for example, can be carried out. See W. W. Wood's review, Chapter 5, in *Physics of Simple Liquids*, edited by H. N. V. Temperley, J. S. Rowlinson and G. S. Rushbrooke (Amsterdam: North-Holland, 1968), Section 4.

(3) If p and T are used as independent variables then the combination $(p\sigma^3/kT)(\epsilon/kT)^{3/n}$ determines the non-ideal part of thermodynamic quantities; if P and V are used the analogous combination is $(PV/N\epsilon)p^{-n/3}$.
(4) Simon, F. E., and Glatze, G., 1929, *Z. Anorg. Allgem. Chem.*, **178,** 309.
(5) Domb, C., 1951, *Phil. Mag.*, **42,** 1316.
(6) Kraut, E. A., and Kennedy, G. C., 1966, *Phys. Rev.*, **151,** 668.
(7) Grover, R. A., 1971, *J. Chem. Phys.*, to be published.
(8) Lindemann, F. A., 1910, *Z. Physik*, **11,** 609.
(9) Ashcroft, N. W., and Lekner, J., 1966, *Phys. Rev.*, **145,** 83; Ashcroft, N. W., and Langreth, D. C., 1967, *Phys. Rev.*, **159,** 500.
(10) Ross, M., 1969, *Phys. Rev.*, **184,** 233.
(11) Alder, B. J., and Wainwright, T. E., 1962, *Phys. Rev.*, **127,** 539.
(12) Metropolis, N. A., Rosenbluth, A. W., Rosenbluth, M. N., Teller, A. H., and Teller, E., 1953, *J. Chem. Phys.*, **21,** 1087; Wood, W. W., and Parker, F. R., 1957, *J. Chem. Phys.*, **27,** 720.
(13) Hoover, W. G., 1971, *J. Chem. Phys.*, to be published.
(14) Hoover, W. G., Ross, M., Johnson, K. W., Henderson, D., Barker, J. A., and Brown, B. C., 1970, *J. Chem. Phys.*, **52,** 4931.
(15) Hoover, W. G., and Ree, F. H., 1968, *J. Chem. Phys.*, **49,** 3609; Alder, B. J., Hoover, W. G., and Young, D. A., 1968, *J. Chem. Phys.*, **49,** 3688.
(16) For an approximate treatment of the effect of surface free energy on the melting transition in computer experiments see J. E. Mayer and W. W. Wood, 1968, *J. Chem. Phys.*, **42,** 4268.
(17) In practice it is easiest to determine the volume at which the (metastable extensions of the) solid and fluid phases have equal Helmholtz free energies, and then to use the equal-area rule to find the pressure corresponding to equal Gibbs free energies.
(18) Wood, W. W., *Physics of Simple Liquids*, edited by H. N. V. Temperley, J. S. Rowlinson and G. S. Rushbrooke (Amsterdam: North-Holland, 1968), p. 116.
(19) Hansen, J.-P., 1970, *Phys. Rev.* A, **2,** 221.
(20) Verlet, L., 1967, *Phys. Rev.*, **159,** 98.
(21) Hansen, J.-P., and Verlet, L., 1969, *Phys. Rev.*, **184,** 151.
(22) Mansoori, G. A., and Canfield, F. B., 1969, *J. Chem. Phys.*, **51,** 4958.
(23) See J. A. Barker, *Lattice Theories of the Liquid State* (Oxford: Pergamon Press, 1963) for a complete discussion of the ideas and thermodynamics of cell theory.
(24) The standard reference is *Dynamical Theory of Crystal Lattices* by M. Born and K. Huang (London: Oxford U.P., 1954).
(25) Squire, D. R., and Salsburg, Z. W., 1961, *J. Chem. Phys.*, **35,** 486.
(26) Alder, B. J., Hoover, W. G., and Wainwright, T. E., 1963, *Phys. Rev. Letters*, **11,** 241.
(27) Alder, B. J., and Wainwright, T. E., 1962, *Phys. Rev.*, **127,** 359.
(28) Ross, M., and Alder, B. J., 1966, *Phys. Rev. Letters*, **16,** 1077.
(29) Ross, M., and Alder, B. J., 1967, *J. Chem. Phys.*, **46,** 4203; Ross, M., and Wackerle, J., to be published.
(30) Stishov, S. M., Makarenko, I. N., Ivanov, V. A., and Fedosimov, V. I., 1970, *JETP Letters*, **11,** 13.